

IKOD: Mitigating Visual Attention Degradation in Large Vision-Language Models

Jiabing Yang^{1,2*}, Chenhang Cui^{3*}, Yiyang Zhou⁴, Yixiang Chen^{1,2}, Peng Xia⁴, Ying Wei⁵, Tao Yu^{1,2}, Yan Huang^{1,2†}, Liang Wang^{1,2}

¹School of Artificial Intelligence, University of Chinese Academy of Sciences

²NLPR, Institute of Automation, Chinese Academy of Sciences

³National University of Singapore ⁴UNC-Chapel Hill ⁵Zhejiang University

yangjiabing2025@ia.ac.cn, yhuang@nlpr.ia.ac.cn

Abstract

Recent advancements in Large Vision-Language Models (LVLMs) have demonstrated significant progress across multiple domains. However, these models still face the inherent challenge of integrating vision and language for collaborative inference, which often leads to “hallucinations”, outputs that are not grounded in the corresponding images. Many efforts have been made to address these issues, but each comes with its own limitations, such as high computational cost or expensive dataset annotation. Recent research shows that LVLMs exhibit a long-term bias where hallucinations increase as the sequence length grows, yet the underlying cause remains poorly understood. Building on extensive research into attention mechanisms in LVLMs, we analyze the relationship between this long-term bias and visual attention. In our research, we identify a consistent phenomenon in current LVLMs: the model’s attention to visual input diminishes as the generated sequence grows, which we hypothesize to be a key factor contributing to observed increasing hallucinations. Based on these insights, we propose **Image** attention-guided **K**ey-value merging **c**ollaborative **D**ecoding (**IKOD**), a collaborative decoding strategy generating more image-focused sequences. This method derives logits from shorter sequences with higher image attention through key-value merging and combines them with those from the original decoding, effectively mitigating attention degradation and suppressing hallucinations while not incurring too much inference cost. Extensive experiments on both hallucination and comprehensive benchmarks demonstrate IKOD’s superior effectiveness in mitigating hallucinations and improving comprehensive capacities for LVLMs. Importantly, IKOD requires no additional training or external tools, making it a lightweight and efficient framework applicable to various models.

1 Introduction

Recent advancements in Large Language Models (LLMs), such as GPT, LLaMA, and Vicuna (Brown et al. 2020; Touvron et al. 2023; Chiang et al. 2023) have profoundly impacted the development of Large Vision-Language Models (LVLMs), enabling significant progress across various domains like literature (Yang et al. 2024), agriculture (Zhu et al. 2024a), visual content generation (Zhu et al. 2024b)

and robotics (Ding et al. 2024). However, LVLMs face inherent limitations in precisely aligning vision and language modalities. These shortcomings can lead to LVLMs’ trustworthy problems like “hallucinations”, where the model generates outputs that are not grounded in the images. These problems have led to significant challenges in critical fields such as finance (Kang and Liu 2023) and medical diagnosis (Chen et al. 2024a), adversely impacting the accuracy and safety of decision-making processes within these systems. Therefore, addressing this issue is crucial for enhancing the performance and reliability of LVLMs.

To address the misalignment between vision and language, a variety of methods have been proposed, including instruction tuning (Liu et al. 2023a; Zhao, Wu, and Huang 2023; Lin et al. 2024a), post-hoc techniques (Zhou et al. 2023; Yin et al. 2024) and contrastive decoding (Leng et al. 2024; Wang et al. 2024; Zhang et al. 2024). While these methods have made great progress, they sometimes rely heavily on additional datasets, external tools, or computational resources. For instance, post-hoc methods depend on external tools such as pre-trained vision-language models (Liu et al. 2024c) and closed-source large models (Brown et al. 2020), which incurs high computational cost and limits their potential for widespread application.

Recent research indicates that LVLMs exhibit a long-term bias where hallucinations increase as sequence grows (Zhou et al. 2023; Favero et al. 2024); however, the underlying causes of this phenomenon remain largely unexplained. Motivated by these findings and prior research on attention mechanisms in large models (Yu, Yu, and Wang 2024; Woo et al. 2024; Zhou et al. 2024a), we aim to analyze the relationship between this long-term bias and visual attention, inspired by the intuition that visual attention partially reflects vision-language alignment, which is closely related to hallucinations. Our observations reveal a consistent phenomenon in current LVLMs: as the generated sequence increases, the LVLMs’ attention to the image gradually diminishes. We refer to this pattern as **Visual Attention Degradation**. Further experiments reveal that this Degradation has a high correlation with increasing hallucinations. Based on these findings, we propose an **Image** attention-guided **K**ey-value merging **c**ollaborative **D**ecoding strategy (**IKOD**), a collaborative decoding strategy that generates image-focused sequences while retaining most of the essential information in the re-

*Equal contribution.

†Corresponding author.

sponse. This approach involves obtaining logits with high image attention from shorter sequences by compressing KV Cache and merging them with the logits derived from the original decoding process, alleviating the decline in visual attention without bringing too much inference cost. Multiple experiments on both hallucination and comprehensive benchmarks demonstrate the effectiveness of IKOD. Another advantage of our method is that it requires no additional training and does not rely on external tools.

Our primary contributions can be summarized as follows:

1. We observe that visual attention degrades as sequence grows in LVLMs, accompanied by increasing hallucinations. We hypothesize that visual attention degradation is a key factor contributing to the hallucinations.
2. Inspired by the insights above, we introduce IKOD, an image attention-guided key-value merging collaborative decoding strategy. This method endows text sequence with high attention on image using key-value merging and collaborates the image-focused decoding process with the original decoding process to obtain a more image-focused output distribution in LVLMs.
3. Comprehensive experiments demonstrate the efficacy of IKOD in mitigating hallucinations and improving visual reasoning. Notably, IKOD requires no additional training or external tools, demonstrating strong applicability.

2 Related Work

Large Vision-Language Models. Recent advances in Large Language Models (LLMs) (Brown et al. 2020; OpenAI 2023; Touvron et al. 2023) have spurred the development of Large Vision-Language Models (LVLMs), which integrate visual features from pre-trained vision models into LLMs’ representation space. LVLMs are typically categorized into MLP-based and QFormer-based architectures and have achieved strong results in image comprehension. However, they remain prone to hallucinations, where generated outputs misrepresent image content. To address this, prior work explores instruction tuning (Lin et al. 2024a; Dai et al. 2024; Liu et al. 2023b), post-processing (Zhou et al. 2023; Yin et al. 2024), preference tuning (Yu et al. 2024a; Zhou et al. 2024b), and decoding strategies (Huang et al. 2024; Chen et al. 2024c). Yet, instruction and preference tuning require costly annotations and intensive computation, while post-processing methods often rely on external tools like powerful vision-language models.

Decoding Strategies for LVLMs. Decoding strategies are crucial for large models, as they determine how the model generates responses based on images and instructions. In addition, they can enhance performance without additional training. They play a pivotal role in shaping output quality, relevance, and coherence. Traditional strategies such as greedy decoding, nucleus sampling, and beam search offer various options for balancing diversity, reliability, and the trade-off between randomness and relevance. Recently, decoding strategies for large foundation models have focused on contrasting logits across layers (Chuang et al. 2023), applying logit penalties (Huang et al. 2024), and employing contrastive decoding (Leng et al. 2024; Chen et al. 2024c).

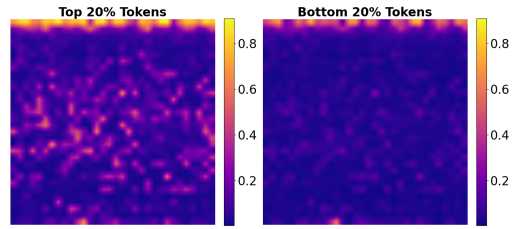


Figure 1: Image attention across different layers and heads of LLaVA-1.5 7B. More examples are in Appendix B.2.

Compared with these methods, our approach mitigates hallucinations via KV Cache compression while striving to minimize the accompanying inference cost.

3 Observations

3.1 Visual Attention Degradation

Visual attention in LVLMs plays a critical role in model performance (Lin et al. 2024b; Yu, Yu, and Wang 2024). Motivated by this, we explore the relationship between visual attention and token positions in generated sequences.

We randomly sample 5,000 images from the MSCOCO validation set using the prompt “*Describe this image in detail.*” For the t -th token in a generated sequence of length L , the attention map at layer i and head j is denoted as: $Att_t^{i,j} \in \mathbb{R}^{1 \times L}$. The total attention to image tokens is calculated by: $Att_{t,image}^{i,j} = \sum_{k \in \text{image_index}} Att_t^{i,j}[k]$, where image_index denotes the indices of image tokens.

We focus on the tokens located in the first and last 20% positions of the generated sequence, defined as $\{1, 2, \dots, \lfloor 0.2L \rfloor\}$ and $\{L - \lfloor 0.2L \rfloor + 1, \dots, L\}$ respectively. The average image attention for the two segments is: $Att_{\text{first}}^{i,j} = \frac{1}{\lfloor 0.2L \rfloor} \sum_{t=1}^{\lfloor 0.2L \rfloor} Att_{t,image}^{i,j}$, $Att_{\text{last}}^{i,j} = \frac{1}{\lfloor 0.2L \rfloor} \sum_{t=L-\lfloor 0.2L \rfloor+1}^L Att_{t,image}^{i,j}$.

As shown in Figure 1, we visualize the attention heatmaps in LLaVA-1.5, where each row corresponds to a transformer layer and each column to an attention head. A clear drop in image attention is observed in the later part of sequences.

To validate this trend, we further visualize the distribution of attention values using kernel density estimation (KDE), as detailed in Appendix B.1. For each token, we compute the averaged image attention across all heads and layers: $Att_{t,image}^{\text{avg}} = \frac{1}{|I||J|} \sum_{i \in I} \sum_{j \in J} Att_{t,image}^{i,j}$, where I and J are the sets of all layers and heads, respectively.

As illustrated in Figure 2, image attention tends to diminish as the sequence grows longer. Additional results across different models are shown in Appendix B.2.

Overall, we identify a consistent pattern in LVLMs: visual attention degrades for later tokens in longer sequences. This may be attributed to the nature of autoregressive generation, where each new token gradually dilutes attention to earlier content. To further explain this, we provide a coarse theoretical analysis based on the following special case. Suppose that the last token x_t (the query) in the se-

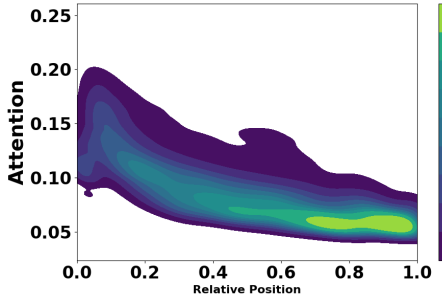


Figure 2: Image attention across different layers and heads of LLaVA-1.5 during response generation, showing the relationship between relative position in the sequence and the average image attention across different heads.

quence attends equally to all previous tokens. Let the lengths of image tokens, generated tokens and other tokens be l_{image} , l_{gen} and l_{others} , respectively. Then, the attention allocated to the image can be computed as:

$$Att_{t,\text{image}}^{i,j} = \frac{l_{\text{image}}}{l_{\text{image}} + l_{\text{others}} + l_{\text{gen}}} \quad (1)$$

Since l_{image} and l_{others} are fixed, the attention to the image decreases as the generated sequence length l_{gen} increases.

3.2 The Relationship Between Visual Attention Degradation and LVLM’s Performance

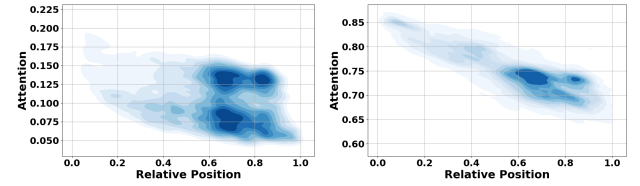
After observing that image attention weakens as the sequence length increases, we are prompted to ask: Does this visual attention degradation affect LVLM performance? To explore this, we analyze its relationship with model hallucinations—instances where the model generates content inconsistent with the input image, often viewed as indicators of degraded performance (Liu et al. 2024b).

We investigate whether reduced attention correlates with hallucinations by visualizing the density distribution of hallucinated tokens across two variables: average image attention and token position, as shown in Figure 3. Experiments are conducted on LLaVA-1.5 and InstructBLIP.

As the sequence progresses, image attention clearly declines. Moreover, hallucinated tokens tend to cluster in low-attention regions, suggesting that lower visual focus may increase the chance of errors. Additional examples are provided in Appendix B.2. ***These observations lead us to hypothesize that visual attention degradation over longer sequences is correlated with increasing hallucinations, potentially resulting in degraded model performance.***

4 Method

In this section, building on previous insights—the degradation of visual attention over longer sequences and its correlation with hallucinations—we propose a lightweight and effective framework IKOD to address these challenges. Section 4.1 reviews the inference process in LVLMs. Section 4.2 introduces the Image Attention-Guided Key-Value Merging Approach designed to reduce the sequence length. Section



(a) LLaVA-1.5 (b) InstructBLIP

Figure 3: Density distribution of the average image attention of hallucinated tokens and their positions on LLaVA-1.5 and InstructBLIP.

4.3 presents a collaborative decoding strategy and Section 4.4 details adaptive plausibility constraints. An overview of our framework is illustrated in Figure 4.

4.1 Preliminary

Large Vision-Language Models (LVLMs) typically comprise three components (Liu et al. 2023b; Dai et al. 2024; Zhu et al. 2023): a vision encoder, a connector, and a language model. Given a visual input v , the encoder extracts features z_v , which are aligned with the instruction x_I via the connector $H(\cdot)$:

$$x_v = H(x_I, z_v), \quad (2)$$

where x_v is the aligned visual embedding. During autoregressive generation, the probability of generating output sequence Y is:

$$p(Y|x, x_v) = \prod_{t=1}^L p(y_t|y_{<t}, x, x_v), \quad (3)$$

where x denotes the text input and L is the length of the generated sequence.

At generation step t , input tokens X_t are projected into query, key, and value vetcors:

$$Q_t = X_t W_Q, \quad K_t = X_t W_K, \quad V_t = X_t W_V,$$

where W_Q , W_K , and W_V are learned matrices. Then self-attention mechanism is adopt as:

$$Z_t = \text{softmax} \left(\frac{Q_t K_t^\top}{\sqrt{d_k}} \right) V_t, \quad (4)$$

followed by residual connection and feed-forward network:

$$Z_{\text{final}} = Z_{\text{prev}} + \text{FFN}(Z_{\text{prev}}). \quad (5)$$

where Z_{prev} is the feature from the previous layers and $\text{FFN}(\cdot)$ is the feed-forward network. Then, we can also model the output distribution as:

$$p(Y|x, x_v) = \prod_{t=1}^L p(y_t|Q_t, K_t, V_t). \quad (6)$$

4.2 Image attention-guided key-value merging

In this section, to ensure that LVLM maintains a strong focus on crucial visual elements and improves the quality of generated text, we propose a key-value merging strategy that

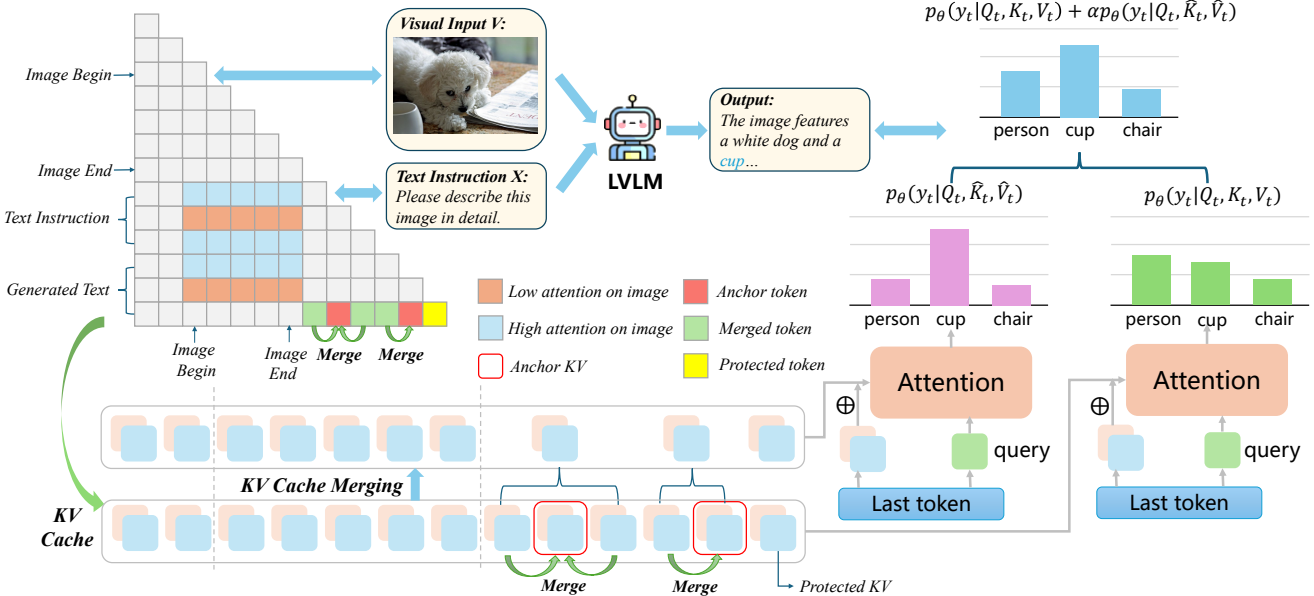


Figure 4: The overall framework of IKOD. We select the tokens with lower attention on image in text sequence to be anchors while merging the remaining tokens’ keys and values (KVs) into the closest anchors’, resulting in a compressed KV Cache namely a shorter contextual sequence with higher attention on image. Then we combine the logits derived from the compressed KV Cache with the original logits to get a output distribution more grounded in image.

shortens the sequence length inspired by KV Cache Management (Zhang et al. 2023; Liu et al. 2024e). This strategy prioritizes visual features by selectively merging key and value vectors of text based on their importance determined by image attention scores. The core idea is to identify anchor points in the key-value vectors that aggregate contextual information. By recognizing the significance of visual attention in Large Vision-Language Models (LVLMs), we can develop policies to predict which vectors in the key-value storage will be most relevant for upcoming inference tasks. This approach helps reduce sequence length and mitigates the problem of diminishing image attention. During the key-value merging stage, this approach involves two primary steps: 1) selecting important key-value anchors based on the layer-wise sum of image attention scores, and 2) merging key-value vectors based on the selected anchors.

Anchors Selection Strategy. Suppose I and J are the sets of model’s all layers and heads, and the text sequence (including instruction and generated tokens) has T tokens. Consider the j -th attention head in the i -th layer, the original key and value are $K^{i,j}$ and $V^{i,j}$, respectively. We can calculate the average attention score for the token x_t in each layer based on the visual attention, denoted as $S_t^i = \frac{1}{|J|} \sum_{j \in J} Att_{t,image}^{i,j}$. Consequently, we obtain independent attention scores for each layer. Since we expect all the tokens in text sequence to have higher attention on image, we pay more attention to the tokens with lower attention scores, which commonly appear at the end of sequence and are more relevant with the query token. Thus we select these tokens as anchors to augment them, while merging the remaining tokens’ keys and values into the closest anchors’. Notably, we

preserve the keys and values of the last token (query token) and its preceding token, given their strong relevance to the current generation step. Given an anchor ratio λ , we select the smallest $K = \lambda \times (T - 2)$ tokens in text sequence (except the two protected tokens) based on their image attention scores in each layer, with the indices $\{t_k^i | k = 1, 2, \dots, K\}$ in ascending order, where i denotes the i -th layer. Taking them as anchors, we have K buckets as:

$$D_k^i = \begin{cases} \{0, \dots, \lfloor \frac{t_1^i + t_2^i}{2} \rfloor\}, & k = 1 \\ \{\lfloor \frac{t_{k-1}^i + t_k^i}{2} \rfloor + 1, \dots, \lfloor \frac{t_k^i + t_{k+1}^i}{2} \rfloor\}, & 1 < k < K \\ \{\lfloor \frac{t_{K-1}^i + t_K^i}{2} \rfloor, \dots, T - 2\}, & k = K \end{cases} \quad (7)$$

where $\lfloor \cdot \rfloor$ denotes the floor function. The division indicates that each token is divided into the closest anchor token’s group across various layer, attributed to the strong contextual associations of close tokens.

Key-Value Merging. When generating the next token, $T+1$, in each layer, we average all the key-value vectors corresponding to each division D_k^i and merge them into $K_{t,k}^{i,j}$ and $V_{t,k}^{i,j}$. Specifically, we compute the averaged key and value vectors for the j -th head of the i -th layer as follows:

$$\tilde{K}_{t,k}^{i,j} = \frac{1}{|D_k^i|} \sum_{m \in D_k^i} K_m^{i,j}, \quad \tilde{V}_{t,k}^{i,j} = \frac{1}{|D_k^i|} \sum_{m \in D_k^i} V_m^{i,j} \quad (8)$$

where D_k^i is the set of all positions in division k for layer i , and $|D_k^i|$ represents the number of elements in that division. Next, we concatenate the averaged key and value vectors across all divisions, along with the previous tokens and

protected tokens, respectively, to obtain the final merged key and value for the j -th head of the i -th layer: $\hat{K}_t^{i,j}$ and $\hat{V}_t^{i,j}$.

This approach allows us to obtain a shorter, more image-focused decoding process by merging keys and values based on image attention, which can be formulated as $p(y_t|y_{<t}, x, x_v) = p_\theta(y_t|Q_t, \hat{K}_t, \hat{V}_t)$. By selectively merging keys and values, it helps the model preserve rich contextual information while increasing the model's focus on visual content.

4.3 Collaborative Decoding

Relying solely on image-focused decoding results in the model failing to fully capture detailed information. The detailed experiment of this issue can be found in Section 5.3. To address this concern, we propose collaborating the original decoding with a shorter sequence decoding that is more focused on the image. This approach is expected to enhance decoding while maintaining the stability of the inference process.

Building on the key-value merging discussed in Section 4.2, we derive the following equation:

$$p(y_t|y_{<t}, x, x_v) = p_\theta(y_t|Q_t, K_t, V_t) + \alpha p_\theta(y_t|Q_t, \hat{K}_t, \hat{V}_t) \quad (9)$$

where α is a hyperparameter that balances the original decoding with the image-focused decoding. By effectively leveraging the collaborative decoding strategy, our method seeks to improve the model's performance, as the integration of original decoding may contribute to alleviating the information loss caused by KV compression.

4.4 Adaptive Plausibility Constraints

Though collaborative decoding based on image attention improves the alignment of LVLMs, a critical challenge remains: the logits of some implausible tokens may be unintentionally amplified. This concern is motivated by the intuition that the tokens with very low probabilities are more likely to be hallucinated and not grounded in the image. Blindly enhancing such tokens may negatively impact generation quality. To address this issue, we draw inspiration from prior works (Li et al. 2023b; Leng et al. 2024) and introduce adaptive plausibility constraints. Specifically, we select next token from those tokens whose probabilities exceed a predefined confidence level in the original output distribution, denoted as follows:

$$\begin{aligned} \mathcal{V}_{\text{head}}(y_{<t}) &= \{y_t \in \mathcal{V} : p(y_t|y_{<t}, x, x_v) \\ &\geq \beta \max_w p(w|y_{<t}, x, x_v)\}, \quad (10) \\ p(y_t|y_{<t}, x, x_v) &= 0, \text{ if } y_t \notin \mathcal{V}_{\text{head}}(y_{<t}) \end{aligned}$$

where \mathcal{V} is the output vocabulary of LVLM and β is a hyperparameter between 0 and 1 to control the truncation of the next token distribution. A larger β means a more strict restriction to the selection of next token, retaining only high-probability tokens.

5 Experiments

In this section, we evaluate IKOD in aligning vision and language modalities in LVLMs and improving the model

Model	Decoding	Random	Popular	Adversarial	Average
LLaVA-1.5	Nucleus	81.07	80.30	77.81	79.73
	Greedy	85.50	84.37	82.32	84.06
	OPERA	84.52	85.38	81.51	83.20
	VCD	<u>87.91</u>	<u>85.83</u>	82.16	<u>85.30</u>
	HALC	84.48	83.53	81.51	83.17
	AGLA	86.32	85.21	83.27	84.93
InstructBLIP	IKOD	89.88	87.86	<u>83.11</u>	86.95
	Nucleus	81.13	78.75	77.83	79.24
	Greedy	86.98	84.31	82.13	84.47
	OPERA	<u>87.12</u>	82.22	80.73	<u>84.54</u>
	VCD	<u>85.72</u>	83.21	81.24	<u>83.39</u>
	HALC	87.05	84.29	<u>82.17</u>	84.50
	AGLA	87.00	<u>84.35</u>	81.86	84.40
	IKOD	87.57	85.15	82.46	85.06

Table 1: F1 score on POPE-MSCOCO dataset. We **Bold** the best results and underline the second best results.

performance. We aim to answer the following questions: (1) Can IKOD reduce hallucination in LVLMs? (2) How does IKOD improve model performance in comprehensive benchmarks? (3) Does the key component of IKOD contribute to the model's performance?

5.1 Experimental Settings

Evaluation Benchmarks. We conduct evaluations on both hallucination benchmarks and comprehensive benchmarks. Specifically, this includes: (1) Hallucination benchmarks (POPE (Li et al. 2023c), CHAIR (Rohrbach et al. 2018)). (2) Comprehensive benchmarks (ScienceQA (SQA) (Lu et al. 2022), MM-Vet (Yu et al. 2024b), MMBench (Liu et al. 2024d), MME (Fu et al. 2024)). More details about these benchmarks are provided in Appendix C.

Baselines. First, we compare our approach with existing decoding methods: Nucleus sampling (top-p = 1.0), Greedy search, OPERA (Huang et al. 2024), VCD (Leng et al. 2024), HALC (Chen et al. 2024c) and AGLA (An et al. 2025). Furthermore, we compare the performance of IKOD with other LVLM preference tuning methods, including Silkie (Li et al. 2023a), LLaVA-RLHF (Sun et al. 2024), and RLHF-V (Yu et al. 2024a). More details about these methods can be found in Appendix D.

Implementation Details. Following previous research (An et al. 2025; Leng et al. 2024), We utilize LLaVA-1.5 (Liu et al. 2024a) and InstructBLIP (Dai et al. 2024) with the language decoder Vicuna 7B as the backbone models. In all experiments, unless specifically mentioned, we adopt Greedy search as the base decoding strategy for IKOD and other methods. The comprehensive parameter settings are detailed in Appendix E. For compared methods, we follow the suggested settings in their respective papers and released codes to ensure a fair comparison. All experiments are conducted on NVIDIA A100 GPUs.

5.2 Main Results

Results on POPE. The prompts used here are in a unified format “*Is there a {object} in the image? Please an-*

Model	Decoding	$C_S \downarrow$	$C_I \downarrow$	R. \uparrow	B-4 \uparrow	Avg. Len
LLaVA-1.5	Nucleus	57.2	14.6	76.5	3.1	105.6
	Greedy	50.0	12.0	81.9	4.8	101.0
	OPERA	48.6	11.2	82.6	4.9	95.2
	VCD	50.8	11.8	81.1	4.5	100.9
	HALC	40.2	8.1	77.1	5.0	94.2
	AGLA	50.0	12.1	81.9	4.8	100.6
	IKOD	36.4	8.8	80.9	5.2	99.5
InstructBLIP	Nucleus	57.6	14.8	71.9	2.8	111.1
	Greedy	46.2	10.4	76.4	4.9	102.4
	OPERA	50.6	12.6	75.9	0.8	97.3
	VCD	52.4	12.2	76.8	4.9	98.6
	HALC	60.2	18.0	74.8	3.9	106.0
	AGLA	46.4	10.4	76.5	5.0	102.4
	IKOD	39.8	6.9	78.8	4.6	119.2

Table 2: Evaluation results on COCO caption benchmark. The maximum generation length is set to 512 across all methods. C_S and C_I correspond to CHAIR_S and CHAIR_I (lower is better). R. and B-4 denote Recall and BLEU-4 (higher is better). Avg. Len indicates the average length of generated sequences.

swer this question with one word.” for all methods. Table 1 presents the results on POPE-MSCOCO dataset (Li et al. 2023c) across various baselines and backbone models. The F1 scores are reported for three distinct task types: Random, Popular, and Adversarial. Notably, significant improvements are observed when comparing IKOD with other methods, thereby underscoring its efficacy in enhancing the performance of LVLMs.

Results on CHAIR. In the CHAIR benchmark, we randomly select 500 images from MSCOCO validation dataset (Lin et al. 2014) to conduct an evaluation. We use a unified prompt “Please describe this image in detail.” for all methods. The results compared with other methods are presented in Table 2. Obviously, IKOD outperforms other approaches on CHAIR_S and CHAIR_I metrics significantly. In BLEU-4 scores and recall scores, IKOD achieves superior performance, effectively improving the accuracy of the generated captions. Moreover, IKOD does not shorten the generated sequence length, demonstrating its ability to preserve diversity in the output. This comparison indicates that IKOD effectively mitigate hallucinations and improve modality alignment in LVLMs. Notably, we alter the prompt and find IKOD shows consistent superiority across different prompts, which can be found in Appendix H.5.

Results on Comprehensive Benchmark. We provide a comparison between IKOD and other approaches on comprehensive benchmarks, as illustrated in Table 3. Without any preference tuning, IKOD still achieves superior performance across multiple comprehensive benchmarks, underscores its exceptional ability to integrate image and text modalities, leading to an enhancement in LVLMs’ visual reasoning. To have a detailed comparison, we evaluate the perception and cognition ability of IKOD and other decoding methods on MME benchmark, where IKOD has a better performance as well. Details are shown in Appendix G.

Method	SQA \uparrow	MM-Vet \uparrow	MMBench \uparrow	MME \uparrow
LLaVA-1.5	66.8	30.5	63.0	1458.8
+ Vffeedback	66.2	31.2	63.9	1432.7
+ Human-Preference	65.8	<u>31.1</u>	60.4	1490.6
+ RLHF-V	<u>67.1</u>	30.9	63.6	1498.3
+ IKOD	68.1	<u>31.1</u>	64.4	<u>1489.4</u>

Table 3: Performance Comparison between IKOD and other preference tuning approaches on comprehensive benchmarks. Some results are cited from Zhou et al. (2024b).

Model	Decoding	POPE \uparrow	$C_S \downarrow$	$C_I \downarrow$	MME \uparrow
LLaVA-1.5	Greedy	85.50	50.0	12.0	1458.79
	IKOD w/o OD	89.07	37.2	8.2	1339.05
	IKOD	89.88	36.4	8.8	1489.41
InstructBLIP	Greedy	86.98	46.2	10.4	1112.59
	IKOD w/o OD	82.91	40.8	6.3	981.24
	IKOD	87.57	39.8	6.9	1132.99

Table 4: Performance comparison of Greedy, IKOD w/o OD and IKOD on POPE-MSCOCO under random setting.

5.3 Ablation Studies

Effect of Collaborative Decoding. To verify the effect of collaborative decoding, we ablate the original decoding from IKOD to get a variant which we call IKOD w/o OD, denoted as:

$$p(y_t | y_{<t}, x, x_v) = p_\theta(y_t | Q_t, \hat{K}_t, \hat{V}_t) \quad (11)$$

since we adopt Greedy Search as the base decoding strategy, the scale factor α is irrelevant to the output and can be removed. We compare the performance of original decoding (Greedy), IKOD w/o OD and IKOD in Table 4. We can see that IKOD w/o OD outperforms Greedy decoding in most cases except on MME. Integrating the original decoding, IKOD shows further performance improvement, especially on MME. A possible reason is that the original method compresses a large number of tokens, which may result in the loss of critical input information, while the integration of original decoding contributes to alleviating it.

Anchor Selection Strategy. In Section 4.2, we select tokens with lower image attention in the text sequence as anchors and merge other tokens’ keys and values into the anchors’. To verify its effectiveness, we conduct an ablation study comparing three anchor selection strategies: randomly selected tokens (Random), high-attention tokens (High Attention), and low-attention tokens (Low Attention (Ours)). Results in Table 5 show that our method achieves the best performance across all anchor ratios. This is reasonable, as tokens with low image attention often appear at the end of the sequence and are more relevant to the query token. Retaining these tokens while merging others retains more contextual information and shortens the sequence, leading to higher average image attention and more faithful generation.

Effect of Anchor Ratio λ . The anchor ratio λ is a key hyperparameter controlling the degree of KV Cache compression. A higher λ retains more tokens with less compression,

Anchor Selection Strategies	0.8	0.6	0.4	0.2
Random	86.84	84.64	83.36	81.53
High Attention	81.33	83.86	83.05	84.79
Low Attention(Ours)	88.37	87.38	89.88	87.60

Table 5: F1 Score comparison of different anchor selection strategies across various anchor ratios on POPE-MSCOCO under random setting.

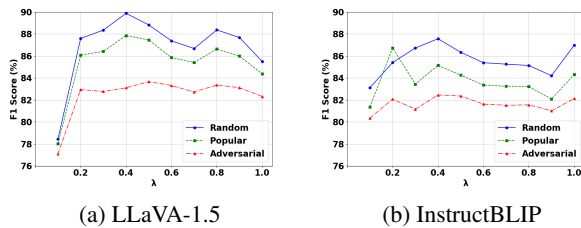


Figure 5: IKOD’s performance on POPE-MSCOCO across different anchor ratios λ on LLaVA-1.5 and InstructBLIP.

and $\lambda = 1$ corresponds to the original full-cache generation. We analyze its effect on POPE-MSCOCO dataset, with results shown in Figure 5. We observe that performance drops when λ is too small or too large, and $\lambda = 0.4$ yields the best results for both LLaVA-1.5 and InstructBLIP. This can be attributed to two factors: (1) A low λ leads to excessive compression and loss of important information; (2) A high λ reduces the benefits of image focus enhanced by KV Cache compression. Based on the results, we set $\lambda = 0.4$ across all experiments unless otherwise specified.

More Ablations. We also conduct ablation studies on the hyperparameters α and β , different sampling strategies, and the scalability of IKOD, which can be found in Appendix H.

5.4 Further Discussions

Inference Cost. As IKOD collaborates two decoding processes during inference, there is a concern about its inference cost. We compare the inference speed of all methods on POPE benchmark, where the number of generated tokens is unified to one for fair comparison. Inference Speed is defined as the average time per item. As shown in Table 6, IKOD achieves competitive speed, outperforming all methods except the original decoding. It slightly surpasses VCD, as both involve dual decoding processes, but IKOD benefits from KV Cache compression in augmented decoding. However, since only text tokens’ KVs are compressed—constituting a relatively small portion of the full sequence—the acceleration is limited. Future work will explore compressing the full sequence for further speedup. A theoretical complexity analysis is provided in Appendix I.

Attention Augmentation Analysis. To visualize the impact of IKOD, we compare the attention maps of IKOD and original LLaVA-1.5 in Figure 6, which reveal the attention scores of generated tokens on image tokens and generated tokens. The horizontal and vertical axes represent the indices of image tokens and generated tokens, respectively. The range of

Method	Greedy	OPERA	VCD	HALC	AGLA	IKOD
Speed (s/item)	0.115	3.015	0.211	3.205	1.589	0.205

Table 6: The Inference Speed comparison between IKOD and other decoding methods on POPE-MSCOCO under random setting.

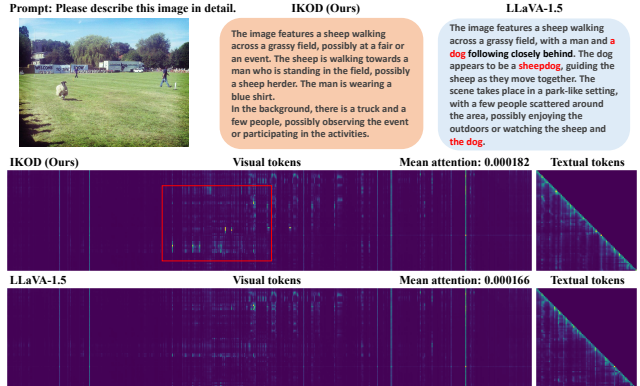


Figure 6: Comparison of attention map between IKOD and LLaVA-1.5 on image caption task. The red box region is labeled with the image attentions that can be significantly improved by IKOD.

values represented by the color scale are unified. We find our method can redirect the LVLM’s attention, helping the model to pay more attention on the visual tokens, leading to the mitigation of internal hallucination patterns. The comparison of mean attention of each generated token on each image token, 0.00182 vs. 0.00166, validates the effect of IKOD’s attention augmentation from a holistic perspective.

Case Studies. We present case studies in Appendix J to further demonstrate the effectiveness of IKOD.

6 Conclusion

In this paper, we investigate the impact of sequence length on image attention in Large Vision-Language Models (LVLMs), specifically focusing on how attention weakens as the sequence grows. Our analysis reveal a significant reduction in image attention towards the end of sequences, which correlates with a higher occurrence of hallucinated tokens and performance degradation in the model. Building on these insights, we introduce IKOD, a lightweight and effective Image attention-guided Key-value merging cOllaborative Decoding strategy, which first enhances the model’s focus on visual elements by selectively merging key and value vectors based on their attention scores, and then combines the image-focused decoding derived from the compressed KV Cache with the original decoding to obtain an output distribution more grounded in the image. Our extensive experiments demonstrate that IKOD can not only mitigate hallucinations in LVLMs but also enhance their comprehensive capacities, avoiding excessive inference cost and eliminating the need for additional training or external tools.

References

An, W.; Tian, F.; Leng, S.; Nie, J.; Lin, H.; Wang, Q.; Chen, P.; Zhang, X.; and Lu, S. 2025. Mitigating object hallucinations in large vision-language models with assembly of global and local attention. In *Proceedings of the Computer Vision and Pattern Recognition Conference*, 29915–29926.

Brown, T.; Mann, B.; Ryder, N.; Subbiah, M.; Kaplan, J. D.; Dhariwal, P.; Neelakantan, A.; Shyam, P.; Sastry, G.; Askell, A.; Agarwal, S.; Herbert-Voss, A.; Krueger, G.; Henighan, T.; Child, R.; Ramesh, A.; Ziegler, D.; Wu, J.; Winter, C.; Hesse, C.; Chen, M.; Sigler, E.; Litwin, M.; Gray, S.; Chess, B.; Clark, J.; Berner, C.; McCandlish, S.; Radford, A.; Sutskever, I.; and Amodei, D. 2020. Language Models are Few-Shot Learners. In Larochelle, H.; Ranzato, M.; Hadsell, R.; Balcan, M.; and Lin, H., eds., *Advances in Neural Information Processing Systems*, volume 33, 1877–1901. Curran Associates, Inc.

Chen, J.; Yang, D.; Wu, T.; Jiang, Y.; Hou, X.; Li, M.; Wang, S.; Xiao, D.; Li, K.; and Zhang, L. 2024a. Detecting and Evaluating Medical Hallucinations in Large Vision Language Models. *CoRR*.

Chen, L.; Zhao, H.; Liu, T.; Bai, S.; Lin, J.; Zhou, C.; and Chang, B. 2024b. An image is worth 1/2 tokens after layer 2: Plug-and-play inference acceleration for large vision-language models. In *European Conference on Computer Vision*, 19–35. Springer.

Chen, Z.; Zhao, Z.; Luo, H.; Yao, H.; Li, B.; and Zhou, J. 2024c. HALC: Object Hallucination Reduction via Adaptive Focal-Contrast Decoding. In *Forty-first International Conference on Machine Learning*.

Chiang, W.-L.; Li, Z.; Lin, Z.; Sheng, Y.; Wu, Z.; Zhang, H.; Zheng, L.; Zhuang, S.; Zhuang, Y.; Gonzalez, J. E.; Stoica, I.; and Xing, E. P. 2023. Vicuna: An Open-Source Chatbot Impressing GPT-4 with 90%* ChatGPT Quality.

Chuang, Y.-S.; Xie, Y.; Luo, H.; Kim, Y.; Glass, J. R.; and He, P. 2023. DoLa: Decoding by Contrasting Layers Improves Factuality in Large Language Models. In *The Twelfth International Conference on Learning Representations*.

Dai, W.; Li, J.; Li, D.; Tiong, A. M. H.; Zhao, J.; Wang, W.; Li, B.; Fung, P. N.; and Hoi, S. 2024. Instructblip: Towards general-purpose vision-language models with instruction tuning. *Advances in Neural Information Processing Systems*, 36.

Ding, Y.; Geng, H.; Xu, C.; Fang, X.; Zhang, J.; Wei, S.; Dai, Q.; Zhang, Z.; and Wang, H. 2024. Open6DOR: Benchmarking open-instruction 6-DoF object rearrangement and a VLM-based approach. In *2024 IEEE/RSJ International Conference on Intelligent Robots and Systems (IROS)*, 7359–7366. IEEE.

Favero, A.; Zancato, L.; Trager, M.; Choudhary, S.; Perera, P.; Achille, A.; Swaminathan, A.; and Soatto, S. 2024. Multi-modal hallucination control by visual information grounding. In *Proceedings of the IEEE/CVF Conference on Computer Vision and Pattern Recognition*, 14303–14312.

Fu, C.; Chen, P.; Shen, Y.; Qin, Y.; Zhang, M.; Lin, X.; Yang, J.; Zheng, X.; Li, K.; Sun, X.; Wu, Y.; and Ji, R. 2024. MME: A Comprehensive Evaluation Benchmark for Multi-modal Large Language Models. *arXiv:2306.13394*.

Huang, Q.; Dong, X.; Zhang, P.; Wang, B.; He, C.; Wang, J.; Lin, D.; Zhang, W.; and Yu, N. 2024. Opera: Alleviating hallucination in multi-modal large language models via over-trust penalty and retrospection-allocation. In *Proceedings of the IEEE/CVF Conference on Computer Vision and Pattern Recognition*, 13418–13427.

Hudson, D. A.; and Manning, C. D. 2019. Gqa: A new dataset for real-world visual reasoning and compositional question answering. In *Proceedings of the IEEE/CVF conference on computer vision and pattern recognition*, 6700–6709.

Kang, H.; and Liu, X.-Y. 2023. Deficiency of large language models in finance: An empirical examination of hallucination. In *I Can't Believe It's Not Better Workshop: Failure Modes in the Age of Foundation Models*.

Leng, S.; Zhang, H.; Chen, G.; Li, X.; Lu, S.; Miao, C.; and Bing, L. 2024. Mitigating object hallucinations in large vision-language models through visual contrastive decoding. In *Proceedings of the IEEE/CVF Conference on Computer Vision and Pattern Recognition*, 13872–13882.

Li, L.; Xie, Z.; Li, M.; Chen, S.; Wang, P.; Chen, L.; Yang, Y.; Wang, B.; and Kong, L. 2023a. Silkie: Preference Distillation for Large Visual Language Models. *CoRR*.

Li, X. L.; Holtzman, A.; Fried, D.; Liang, P.; Eisner, J.; Hashimoto, T.; Zettlemoyer, L.; and Lewis, M. 2023b. Contrastive Decoding: Open-ended Text Generation as Optimization. In *The 61st Annual Meeting Of The Association For Computational Linguistics*.

Li, Y.; Du, Y.; Zhou, K.; Wang, J.; Zhao, X.; and Wen, J.-R. 2023c. Evaluating Object Hallucination in Large Vision-Language Models. In Bouamor, H.; Pino, J.; and Bali, K., eds., *Proceedings of the 2023 Conference on Empirical Methods in Natural Language Processing*, 292–305. Singapore: Association for Computational Linguistics.

Lin, J.; Yin, H.; Ping, W.; Molchanov, P.; Shoeybi, M.; and Han, S. 2024a. Vila: On pre-training for visual language models. In *Proceedings of the IEEE/CVF conference on computer vision and pattern recognition*, 26689–26699.

Lin, T.-Y.; Maire, M.; Belongie, S.; Hays, J.; Perona, P.; Ramanan, D.; Dollár, P.; and Zitnick, C. L. 2014. Microsoft coco: Common objects in context. In *Computer Vision–ECCV 2014: 13th European Conference, Zurich, Switzerland, September 6–12, 2014, Proceedings, Part V 13*, 740–755. Springer.

Lin, Z.; Lin, M.; Lin, L.; and Ji, R. 2024b. Boosting Multimodal Large Language Models with Visual Tokens Withdrawal for Rapid Inference. *arXiv preprint arXiv:2405.05803*.

Liu, F.; Lin, K.; Li, L.; Wang, J.; Yacoob, Y.; and Wang, L. 2023a. Aligning large multi-modal model with robust instruction tuning. *CoRR*.

Liu, H.; Li, C.; Li, Y.; and Lee, Y. J. 2024a. Improved baselines with visual instruction tuning. In *Proceedings of the IEEE/CVF Conference on Computer Vision and Pattern Recognition*, 26296–26306.

Liu, H.; Li, C.; Wu, Q.; and Lee, Y. J. 2023b. Visual Instruction Tuning. In *Thirty-seventh Conference on Neural Information Processing Systems*.

Liu, H.; Xue, W.; Chen, Y.; Chen, D.; Zhao, X.; Wang, K.; Hou, L.; Li, R.; and Peng, W. 2024b. A survey on hallucination in large vision-language models. *arXiv preprint arXiv:2402.00253*.

Liu, S.; Zeng, Z.; Ren, T.; Li, F.; Zhang, H.; Yang, J.; Jiang, Q.; Li, C.; Yang, J.; Su, H.; et al. 2024c. Grounding dino: Marrying dino with grounded pre-training for open-set object detection. In *European Conference on Computer Vision*, 38–55. Springer.

Liu, Y.; Duan, H.; Zhang, Y.; Li, B.; Zhang, S.; Zhao, W.; Yuan, Y.; Wang, J.; He, C.; Liu, Z.; et al. 2024d. Mmbench: Is your multi-modal model an all-around player? In *European conference on computer vision*, 216–233. Springer.

Liu, Z.; Liu, B.; Wang, J.; Dong, Y.; Chen, G.; Rao, Y.; Krishna, R.; and Lu, J. 2024e. Efficient inference of vision instruction-following models with elastic cache. In *European Conference on Computer Vision*, 54–69. Springer.

Lu, P.; Mishra, S.; Xia, T.; Qiu, L.; Chang, K.-W.; Zhu, S.-C.; Tafjord, O.; Clark, P.; and Kalyan, A. 2022. Learn to explain: Multimodal reasoning via thought chains for science question answering. *Advances in Neural Information Processing Systems*, 35: 2507–2521.

OpenAI. 2023. GPT-4 Technical Report. *ArXiv*, abs/2303.08774.

Rohrbach, A.; Hendricks, L. A.; Burns, K.; Darrell, T.; and Saenko, K. 2018. Object Hallucination in Image Captioning. In Riloff, E.; Chiang, D.; Hockenmaier, J.; and Tsujii, J., eds., *Proceedings of the 2018 Conference on Empirical Methods in Natural Language Processing*, 4035–4045. Brussels, Belgium: Association for Computational Linguistics.

Schwenk, D.; Khandelwal, A.; Clark, C.; Marino, K.; and Mottaghi, R. 2022. A-okvqa: A benchmark for visual question answering using world knowledge. In *European conference on computer vision*, 146–162. Springer.

Sun, Z.; Shen, S.; Cao, S.; Liu, H.; Li, C.; Shen, Y.; Gan, C.; Gui, L.-Y.; Wang, Y.-X.; Yang, Y.; et al. 2024. Aligning Large Multimodal Models with Factually Augmented RLHF. In *Annual Meeting of the Association for Computational Linguistics*.

Touvron, H.; Lavril, T.; Izacard, G.; Martinet, X.; Lachaux, M.-A.; Lacroix, T.; Rozière, B.; Goyal, N.; Hambro, E.; Azhar, F.; et al. 2023. Llama: Open and efficient foundation language models. *arXiv preprint arXiv:2302.13971*.

Wang, X.; Pan, J.; Ding, L.; and Biemann, C. 2024. Mitigating Hallucinations in Large Vision-Language Models with Instruction Contrastive Decoding. In *ACL (Findings)*.

Woo, S.; Kim, D.; Jang, J.; Choi, Y.; and Kim, C. 2024. Don’t Miss the Forest for the Trees: Attentional Vision Calibration for Large Vision Language Models. *CoRR*.

Yang, S.; Ge, Y.; Li, Y.; Chen, Y.; Ge, Y.; Shan, Y.; and Chen, Y. 2024. SEED-Story: Multimodal Long Story Generation with Large Language Model. *CoRR*.

Yin, S.; Fu, C.; Zhao, S.; Xu, T.; Wang, H.; Sui, D.; Shen, Y.; Li, K.; Sun, X.; and Chen, E. 2024. Woodpecker: Hallucination correction for multimodal large language models. *Science China Information Sciences*, 67(12): 220105.

Yu, R.; Yu, W.; and Wang, X. 2024. Attention prompting on image for large vision-language models. In *European Conference on Computer Vision*, 251–268. Springer.

Yu, T.; Yao, Y.; Zhang, H.; He, T.; Han, Y.; Cui, G.; Hu, J.; Liu, Z.; Zheng, H.-T.; Sun, M.; et al. 2024a. Rlhf-v: Towards trustworthy mllms via behavior alignment from fine-grained correctional human feedback. In *Proceedings of the IEEE/CVF Conference on Computer Vision and Pattern Recognition*, 13807–13816.

Yu, W.; Yang, Z.; Li, L.; Wang, J.; Lin, K.; Liu, Z.; Wang, X.; and Wang, L. 2024b. MM-Vet: Evaluating Large Multimodal Models for Integrated Capabilities. In *Forty-first International Conference on Machine Learning*.

Zhang, Y.-F.; Yu, W.; Wen, Q.; Wang, X.; Zhang, Z.; Wang, L.; Jin, R.; and Tan, T. 2024. Debiasing Multimodal Large Language Models. *CoRR*.

Zhang, Z.; Sheng, Y.; Zhou, T.; Chen, T.; Zheng, L.; Cai, R.; Song, Z.; Tian, Y.; Ré, C.; Barrett, C.; et al. 2023. H2o: Heavy-hitter oracle for efficient generative inference of large language models. *Advances in Neural Information Processing Systems*, 36: 34661–34710.

Zhao, B.; Wu, B.; and Huang, T. 2023. SVIT: Scaling up Visual Instruction Tuning. *CoRR*.

Zhou, G.; Yan, Y.; Zou, X.; Wang, K.; Liu, A.; and Hu, X. 2024a. Mitigating Modality Prior-Induced Hallucinations in Multimodal Large Language Models via Deciphering Attention Causality. *arXiv preprint arXiv:2410.04780*.

Zhou, Y.; Cui, C.; Rafailov, R.; Finn, C.; and Yao, H. 2024b. Aligning Modalities in Vision Large Language Models via Preference Fine-tuning. In *ICLR 2024 Workshop on Reliable and Responsible Foundation Models*.

Zhou, Y.; Cui, C.; Yoon, J.; Zhang, L.; Deng, Z.; Finn, C.; Bansal, M.; and Yao, H. 2023. Analyzing and Mitigating Object Hallucination in Large Vision-Language Models. In *The Twelfth International Conference on Learning Representations*.

Zhu, D.; Chen, J.; Shen, X.; Li, X.; and Elhoseiny, M. 2023. MiniGPT-4: Enhancing Vision-Language Understanding with Advanced Large Language Models. In *The Twelfth International Conference on Learning Representations*.

Zhu, H.; Qin, S.; Su, M.; Lin, C.; Li, A.; and Gao, J. 2024a. Harnessing Large Vision and Language Models in Agriculture: A Review. *arXiv preprint arXiv:2407.19679*.

Zhu, Y.; Liu, J.; Gao, F.; Liu, W.; Wang, X.; Wang, P.; Huang, F.; Yao, C.; and Yang, Z. 2024b. Visual Text Generation in the Wild. In *European Conference on Computer Vision*, 89–106.

A Limitations and Future Work

Though there are many strengths for IKOD, we still acknowledge that it has some limitations. As we obtain an augmented view on input image through key-value merging, it's not always beneficial in some cases. When the input image has some misleading information, excessive focus on the image could make models prone to generating responses that go against common sense. Moreover, the hyperparameter α modulating the balance of augmented and original output distributions and the anchor ratio λ controlling the degree of KV Cache compression need to be set manually, which limits its convenience to some extent. Exploring self-adaptive methods to replace them will be left for future study. In addition, though we select two representative LVLMs as the base models, the family of LVLMs is so big that we will try to apply IKOD to other LVLMs to further demonstrate its versatility.

B Implementation about the Visualization

B.1 Details about the visualization metric

KDE is a non-parametric way to estimate the probability density function of a random variable by smoothing out the data points. The idea behind KDE is to estimate the distribution of data points by placing a kernel function on each data point and summing them up to create a smooth estimate of the data's probability density. For two-dimensional data x and y , the KDE is defined by the following formula:

$$\hat{f}(x, y) = \frac{1}{nh_x h_y} \sum_{i=1}^n K\left(\frac{x - x_i}{h_x}, \frac{y - y_i}{h_y}\right), \quad (12)$$

where:

- $\hat{f}(x, y)$ is the estimated density at the point (x, y) .
- n is the number of data points.
- $K(\cdot)$ is the kernel function, typically a Gaussian kernel:

$$K(u, v) = \frac{1}{2\pi} e^{-\frac{1}{2}(u^2 + v^2)}$$

- h_x and h_y are the bandwidth parameters, which control the smoothness of the density estimate. We set both h_x and h_y to 0.5 in our analysis.

B.2 More examples of visualization of attention in LVLMs

We conduct an analysis on the relationship between image attention and token position across different Large Vision-Language Models (LVLMs), as well as the relationship between image attention and model performance. We present the visualization in Figure 7. A similar phenomenon is observed across different models: as the sequence length increases, image attention diminishes, particularly towards tokens appearing later in the sequence. Also, we find that weakened attention is correlated with a higher concentration of hallucinated tokens in areas with low attention, indicating that reducing image attention is more likely to lead to errors in LVLMs.

C Evaluation Metrics and Benchmarks

POPE. The Polling-based Object Probing Evaluation (POPE) (Li et al. 2023c) is a widely-used benchmark to assess object hallucination in LVLMs, which contains 27,000 Yes/No questions in three datasets: MSCOCO (Lin et al. 2014), A-OKVQA (Schwenk et al. 2022), GQA (Hudson and Manning 2019). Each dataset has three negative sample settings: random, popular, adversarial. It adopts Accuracy, Precision, Recall, and F1 score as evaluation metrics.

CHAIR. Caption Hallucination Assessment with Image Relevance (CHAIR) (Rohrbach et al. 2018) is a popular method to evaluate object hallucination in image caption tasks. It compares generated objects with ground-truth objects to calculate the degree of hallucination. CHAIR evaluate object hallucination from two dimensions: instance-level and sentence-level, denoted as CHAIR_I and CHAIR_S respectively, which are computed as:

$$\text{CHAIR}_I = \frac{|\{\text{hallucinated objects}\}|}{|\{\text{all mentioned objects}\}|}$$

$$\text{CHAIR}_S = \frac{|\{\text{captions with hallucinated objects}\}|}{|\{\text{all captions}\}|}$$

SQA. ScienceQA (SQA) (Lu et al. 2022) is a benchmark that consists of 21k multimodal multiple choice questions within the science domain, along with annotations of their answers and corresponding lectures and explanations.

MM-Vet. MM-Vet (Yu et al. 2024b) is an evaluation benchmark to assess the performance of LVLMs on complicated multimodal tasks, which focus on six core vision-language capabilities: recognition, knowledge, optical character recognition (OCR), spatial awareness, language generation, and math.

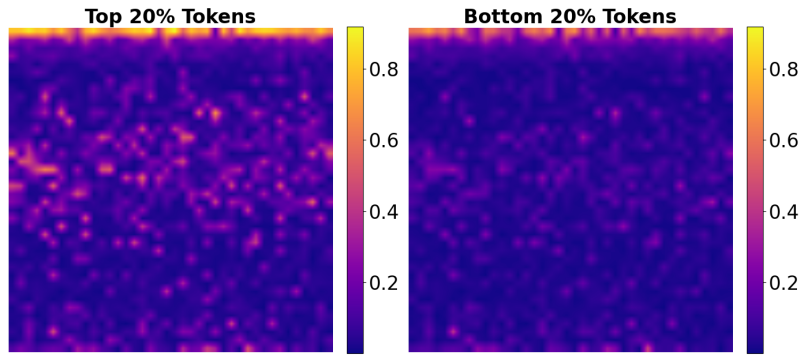
MMBench. MMBench (Liu et al. 2024d) is a meticulously curated dataset expanding the scope of evaluation questions and abilities. It introduces a rigorous CircularEval strategy which leverages large language models to convert free-form predictions into predefined choices, resulting in more accurate evaluation results.

MME. Multimodal Large Language Model Evaluation (MME) (Fu et al. 2024) is a comprehensive benchmark to assess the capabilities of LVLMs in multimodal tasks. It evaluates models with the total score of Accuracy and Accuracy+ across two primary dimensions: perception and cognition, containing 10 and 4 meticulously designed subtasks, respectively.

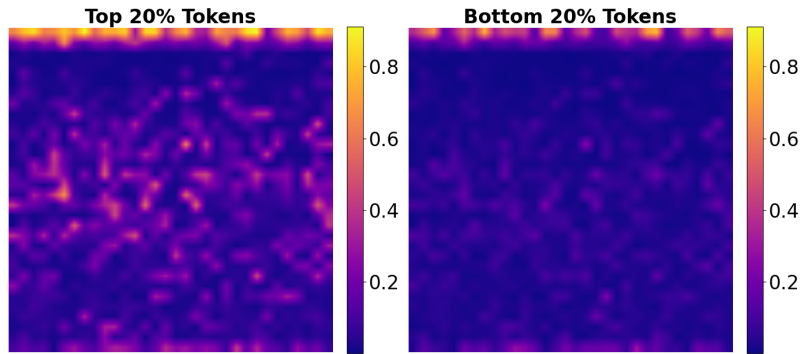
D Overview of the Baselines

LLaVA-1.5. LLaVA-1.5 (Liu et al. 2024a) is an improvement based on LLaVA (Liu et al. 2023b). It modifies with a CLIP-ViT-L-336px visual backbone and MLP projection and incorporates academic task-oriented VQA data with response formatting prompts, achieving state-of-the-art across 11 benchmarks at that time.

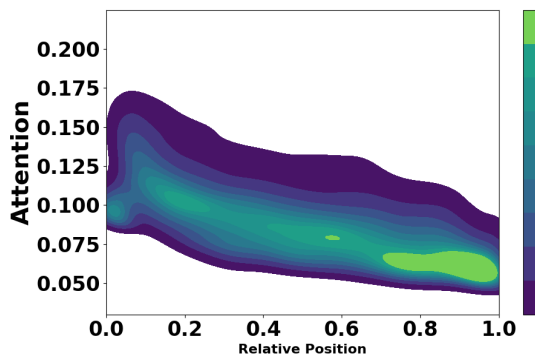
InstructBLIP. InstructBLIP (Dai et al. 2024) utilizes an instruction-aware Query Transformer to extract informative features tailored to the given instruction, demonstrating significant instruction following ability. It achieves state-of-the-



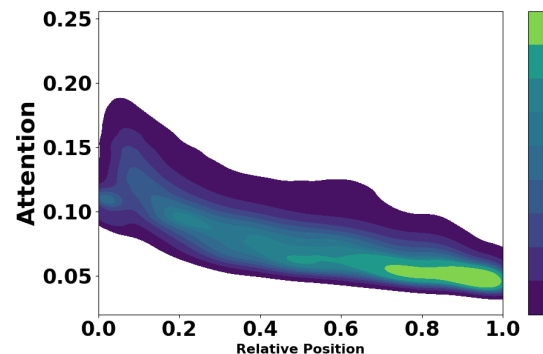
(a) Image attention across different layers and heads in svit 13B.



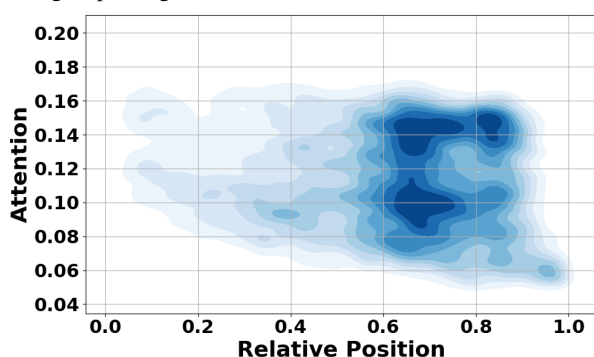
(b) Image attention across different layers and heads in VILA 7B.



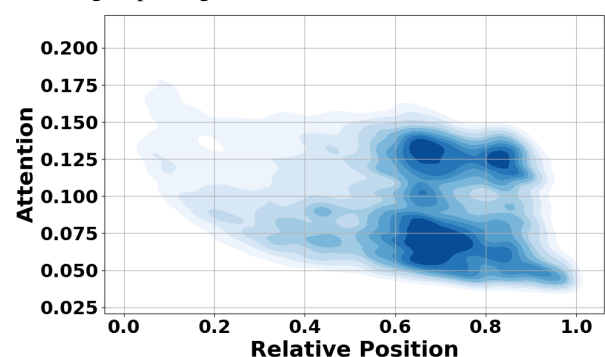
(c) Image attention across different layers and heads of svit 13B during response generation.



(d) Image attention across different layers and heads of VILA 7B during response generation.



(e) Relationship between image attention and model performance on svit.



(f) Relationship between image attention and model performance on VILA.

Figure 7: More examples of attention visualization.

art zero-shot performance across 13 datasets and also excels in some finetuned downstream tasks, like ScienceQA.

OPERA. OPERA (Huang et al. 2024) is a novel MLLM decoding method based on an Over-trust Penalty and a Retrospection-Allocation strategy. It adds a penalty to the model logits to mitigate the over-trust issue on summary token, along with a rollback strategy to correct the token selection.

VCD. Visual Contrastive Decoding (VCD) (Leng et al. 2024) calibrates model’s outputs through contrasting output distributions derived from original and distorted visual inputs, thus reducing the the over-reliance on statistical bias and unimodal priors, significantly mitigating the object hallucination issue across different LVLMs.

HALC. HALC (Chen et al. 2024c) is a plug-and-play decoding algorithm to mitigate object hallucination in LVLMs. It operates on both local and global contexts, integrating a robust auto-focal grounding mechanism to correct hallucinated tokens and a specialized beam search algorithm promoting further visually matched generations.

AGLA. AGLA (An et al. 2025) leverages an image-prompt matching scheme to get an augmented view of the input image where prompt-relevant content is reserved while others are masked. With the augmented view, models can calibrate the output distribution by integrating generative global features and discriminative local features.

Silkie. Silkie (Li et al. 2023a) uses AI annotation to build a vision-language feedback (VLFeedback) dataset. With preference distillation through direct preference optimization (DPO) on it, Silkie achieves more comprehensive improvements compared to human-annotated preference datasets.

LLaVA-RLHF. LLaVA-RLHF (Sun et al. 2024) introduces Reinforcement Learning from Human Feedback (RLHF) from the text domain to the task of vision-language alignment. With the proposed Factually Augmented RLHF, it augments the reward model with additional factual information and alleviates the reward hacking phenomenon in RLHF, resulting in a performance improvement.

RLHF-V. RLHF-V (Yu et al. 2024a) collects human preference at segment-level and performs dense direct preference optimization on it, achieving state-of-the-art performance in trustworthiness among open-source LVLMs at that time.

E Experimental Settings

Most hyperparameters are set based on Grid Search. In all experimental setups, we fix the anchor ratio λ to 0.4 and β to 0.1 unless explicitly stated otherwise. For POPE and CHAIR, We set α to 2 for LLaVA-1.5, while setting α to 1.1 for InstructBLIP. For MME, α is uniformly set to 0.8, while λ is set to 0.9 for LLaVA-1.5 and 0.8 for InstructBLIP, respectively. For other benchmarks, the hyperparameters are the same as POPE’s on LLaVA-1.5. Further optimization of λ , α , β may yield better results. The current settings serve as a baseline to demonstrate the efficacy of our approach.

F POPE Experiment Details

We show the full results on POPE-MSCOCO dataset in Table 7. From the table, we can see that the proposed decod-

ing strategy IKOD consistently outperforms other methods in terms of accuracy and F1 Score across nearly all settings, especially under random setting, demonstrating the significant strength of our method. Though we do not achieve the best performance on adversarial setting, which may be attributed to the frequent co-occurrence schemes in pretrained datasets and our excessive attention on image, IKOD still gains the suboptimal results, proving its superiority.

G MME Experiment Details

To compare the performance of IKOD and other decoding methods, we conduct comprehensive experiments on MME benchmark based on the backbones of LLaVA-1.5 and InstructBLIP. As illustrated in Table 8 and 9, our method achieves the best performance on perception capability and suboptimal results on cognition capability for LLaVA-1.5. For InstructBLIP, despite IKOD lags behind VCD in perception capability, it surpasses all other methods on cognition capability, further demonstrating its effectiveness in improving LVLMs’ comprehensive capacities. As for the subtasks, each method has its own advantages, we do not make a specific comparison.

H Ablation Studies

H.1 Effect of α

α is an important hyperparameter which modulates the level of amplification between original and augmented output distributions, as formulated in Equation 9. Figure 8 demonstrates the results of an ablation study focusing on α , from where we can observe the trend of model’s performance increasing first and then decreasing as α grows, and the best α are 2 and 1.1 for LLaVA-1.5 and InstructBLIP, respectively. When α is small, the effect of amplification is not obvious. Conversely, too large α could break the balance of original and augmented output distribution, distorting model’s inherent parameter information.

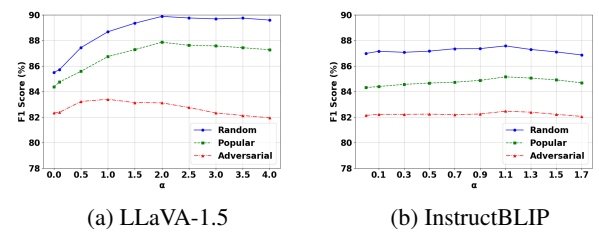


Figure 8: IKOD’s performance on POPE-MSCOCO dataset across different α on LLaVA-1.5 and InstructBLIP.

H.2 Effect of β

β controls the adaptive plausible constraints in Equation 11. As the constraint is set based on the max logit of candidate tokens, it may not work for greedy decoding. So we adopt nucleus sampling (top-p = 1.0) to explore the effect of β . The ablation results are shown in Figure 9. $\beta = 0$, implying no constraint, has suboptimal performance, validating our

Table 7: POPE results on MSCOCO dataset. Higher accuracy and F1 score indicate better performance. **Bold** indicates the best results of all methods.

Setting	Model	Decoding	Accuracy	Precision	Recall	F1 Score
Random	LLaVA-1.5	Nucleus	82.97	91.24	72.93	81.07
		Greedy	87.07	97.28	76.27	85.50
		OPERA	86.30	97.14	74.80	84.52
		VCD	88.37	91.49	84.60	87.91
		HALC	86.27	97.14	74.73	84.48
		AGLA	87.73	97.56	77.40	86.32
		IKOD	90.17	92.58	87.33	89.88
Popular	InstructBLIP	Nucleus	81.37	82.07	80.27	81.16
		Greedy	87.97	94.81	80.33	86.97
		OPERA	88.07	94.61	80.73	87.12
		VCD	86.77	93.05	79.47	85.72
		HALC	88.03	94.82	80.47	87.05
		AGLA	88.00	94.88	80.33	87.00
		IKOD	88.23	92.77	82.93	87.57
Adversarial	LLaVA-1.5	Nucleus	82.10	89.31	72.93	80.30
		Greedy	85.87	84.39	76.27	84.37
		OPERA	85.30	94.68	74.80	85.38
		VCD	86.03	87.10	84.60	85.83
		HALC	85.27	94.68	74.73	83.53
		AGLA	86.57	94.78	77.40	85.21
		IKOD	87.93	88.39	87.33	87.86
Popular	InstructBLIP	Nucleus	79.23	78.46	80.60	79.51
		Greedy	85.00	88.60	80.33	84.27
		OPERA	84.93	88.14	80.73	84.27
		VCD	83.97	87.33	79.47	83.21
		HALC	85.00	88.49	80.47	84.29
		AGLA	85.10	88.80	80.33	84.35
		IKOD	85.53	87.48	82.93	85.15
Adversarial	LLaVA-1.5	Nucleus	79.20	83.38	72.93	77.81
		Greedy	83.63	89.51	76.20	82.32
		OPERA	83.07	89.74	74.67	81.51
		VCD	81.63	79.86	84.60	82.16
		HALC	83.07	89.81	74.60	81.51
		AGLA	84.47	90.20	77.33	83.27
		IKOD	82.27	79.33	87.27	83.11
Popular	InstructBLIP	Nucleus	77.40	76.08	79.93	77.96
		Greedy	82.47	83.77	80.53	82.12
		OPERA	82.51	83.55	80.93	82.22
		VCD	81.63	83.02	79.53	81.24
		HALC	82.50	83.74	80.67	82.17
		AGLA	82.17	83.30	80.47	81.86
		IKOD	82.33	81.87	83.07	82.46

rationale for implementing this constraint. For LLaVA-1.5, F1 score increases first and then decreases as β increases, while for InstructBLIP, F1 score grows continuously, indicating that the best threshold for the constraint is low for LLaVA-1.5 and high for InstructBLIP. Too large β may unexpectedly exclude valid tokens. When applied, we encourage users to set it to a rational value, such as 0.1.

H.3 Effect of Different Sampling Strategies

Following VCD’s setting (Leng et al. 2024), we conduct an ablation study on various sampling strategies using POPE-

MSCOCO dataset under the random setting with LLaVA-1.5 backbone. In addition to the greedy search approach discussed in the main paper, this experiment includes four additional sampling strategies: Top P sampling (specifically, top-p = 0.9), Top K sampling (specifically, top-k = 50), Nucleus sampling (top-p = 1.0), and Top K sampling with temperature normalization (top-k = 50, temperature = 0.7/1.5). Results are presented in Table 10. We can observe that applying IKOD, irrespective of the sampling strategy employed, consistently contributes to the mitigation of hallucinations in LLMs. This consistency underscores the versa-

Model	Decoding	Existence	Count	Position	Color	Posters	Celebrity	Scene	Landmark	Artwork	OCR	Perception Total
LLaVA-1.5	Nucleus	180.00	101.67	111.67	140.00	105.10	111.76	144.50	122.50	101.75	100.00	1218.95
	Greedy	195.00	158.33	123.33	155.00	129.59	133.53	154.75	163.25	121.00	125.00	1458.79
	VCD	185.00	153.33	133.33	138.33	130.27	152.94	148.25	166.00	123.50	130.00	1460.96
	AGLA	195.00	155.00	133.33	160.00	142.86	133.53	156.25	164.50	114.50	132.50	1487.47
	IKOD	195.00	173.33	128.33	160.00	129.59	137.65	156.50	159.25	117.25	132.50	1489.41
InstructBLIP	Nucleus	168.33	51.67	56.67	115.00	117.01	97.65	147.00	132.75	92.75	80.00	1058.82
	Greedy	185.00	60.00	50.00	120.00	141.84	80.00	160.00	159.25	91.50	65.00	1112.59
	VCD	185.00	60.00	51.67	123.33	150.68	97.65	156.50	161.50	96.00	102.50	1184.83
	AGLA	185.00	60.00	50.00	120.00	141.84	82.65	160.50	160.00	91.50	65.00	1116.48
	IKOD	185.00	55.00	48.33	105.00	156.80	92.35	159.50	154.25	89.25	87.50	1132.99

Table 8: Results on MME cognition-related tasks.

Model	Decoding	Common Sense Reasoning	Numerical Calculation	Text Translation	Code Reasoning	Cognition Total
LLaVA-1.5	Nucleus	107.86	60.00	57.50	97.50	322.86
	Greedy	120.71	50.00	50.00	77.50	298.21
	VCD	120.71	47.50	57.50	72.50	298.21
	AGLA	115.00	37.50	50.00	62.50	265.00
	IKOD	120.00	55.00	57.50	67.50	300.00
InstructBLIP	Nucleus	72.86	90.00	50.00	40.00	252.86
	Greedy	97.86	47.50	50.00	45.00	240.36
	VCD	102.14	45.00	57.50	47.50	252.14
	AGLA	97.86	47.50	50.00	45.00	240.36
	IKOD	99.29	42.50	70.00	45.00	256.79

Table 9: Results on MME perception-related tasks.

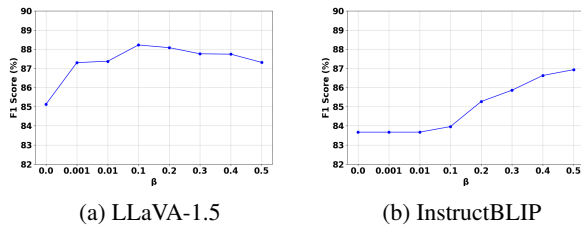


Figure 9: IKOD’s performance on POPE-MSCOCO under random setting across different β on LLaVA-1.5 and InstructBLIP.

tility and effectiveness of IKOD in enhancing the alignment of vision and language in LVLMs.

H.4 Effect of IKOD when LVLMs Scale Up

To assess the scalability of IKOD, we extend the evaluation to larger 13B variants of LLaVA-1.5 and InstructBLIP. We adopt Greedy Search as the base decoding strategy, and the results are revealed in Table 11. Obviously, when models are scaled up, IKOD consistently boosts the performance in addressing the hallucination issue, affirming its robustness independent of model scale.

H.5 Effect of Different Prompts

In the main experiments, we utilize “*Please describe this image in detail.*” as the prompt to evaluate IKOD on CHAIR benchmark. To explore the stability of IKOD across different prompts, we design another three prompt variants, which are revealed in Table 12. Although these three prompts have similar semantics, the sequences derived from them have significantly different lengths. Despite the discrepancy, our method shows a consistent improvement in mitigating hallucinations in almost all cases, verifying the stability of its effectiveness across different prompts. Recall and BLEU-4 are strongly influenced by the sequence length, so we only include them here for reference.

I Computational Complexity

Here we theoretically analyze the computational complexity of IKOD. We only consider the forward computation of multi-head attention (MHA) and feed-forward network(FFN) module in the FLOPs estimation to make a simplification. The original floating-point operations (FLOPs) required can be expressed as:

$$\text{Original_FLOPs} = L \times (24nd^2 + 4n^2d), \quad (13)$$

where L denotes the number of transformer layers, n is the sequence length, d represents the hidden dimension size. This equation highlights the significant impact of sequence length n on computational complexity. Following

Sampling Strategy	w. IKOD	Accuracy	Precision	Recall		F1 Score
Top P	No	86.63	96.14	76.33		85.10
	Yes	89.60	91.17	87.07		89.33
Top K	No	82.97	91.24	72.93		81.07
	Yes	88.53	90.99	85.53		88.18
Nucleus	No	82.97	91.24	72.93		81.07
	Yes	88.57	91.00	85.60		88.22
Top K+Temperature 0.7	No	86.93	96.63	76.53		85.42
	Yes	89.97	92.07	87.47		89.71
Top K+Temperature 1.5	No	86.27	95.26	76.33		84.75
	Yes	89.47	91.75	86.73		89.17

Table 10: An ablation study of different sampling strategies on POPE benchmark.

Dataset	POPE	Model	Decoding	Accuracy	Precision	Recall	F1 Score
Random	LLaVA-1.5 (13B)	Greedy	86.67	97.41	75.33	84.96	
		IKOD	87.40	97.22	77.00		85.94
	InstructBLIP (13B)	Greedy	88.10	95.90	79.60	86.99	
	InstructBLIP (13B)	IKOD	89.80	89.48	90.20		89.84
MSCOCO		Greedy	85.97	95.68	75.33	84.30	
LLaVA-1.5 (13B)	IKOD	86.37	94.68	77.07		84.97	
	Greedy	85.57	90.39	79.60	84.65		
Popular	InstructBLIP (13B)	IKOD	86.47	87.89	85.32		86.59
		Greedy	84.20	91.71	75.20	82.64	
	InstructBLIP (13B)	IKOD	84.20	90.14	76.8		82.94
Adversarial	LLaVA-1.5 (13B)	Greedy	82.87	85.26	79.47	82.26	
		IKOD	83.63	76.74	90.13		82.90

Table 11: Results of 13B-sized LLaVA-1.5 and InstructBLIP variants on POPE benchmark.

Prompt	Model	Decoding	CHAIR _S ↓	CHAIR _I ↓	Recall ↑	BLEU-4 ↑	Avg. Len
Describe this image.	LLaVA-1.5	Greedy	48.6	11.7	81.5	4.7	99.6
		IKOD	35.0	8.0	80.0	5.3	95.6
	InstructBLIP	Greedy	19.0	5.4	62.3	8.3	56.2
Generate a caption for this image.	LLaVA-1.5	Greedy	13.4	6.9	56.4	16.7	24.5
		IKOD	9.8	5.6	51.6	22.0	18.7
	InstructBLIP	Greedy	5.8	3.9	47.5	41.6	9.7
What is showing in this image?	LLaVA-1.5	Greedy	9.8	5.5	49.0	19.0	20.5
		IKOD	9.2	5.2	48.3	18.4	21.6
	InstructBLIP	Greedy	25.8	8.5	65.0	11.2	44.9
	IKOD	17.2	6.7	61.8	13.9	35.1	

Table 12: An ablation study of different prompts on CHAIR benchmark.

FastV (Chen et al. 2024b), we make a rough estimation of IKOD’s FLOPs as follows:

where \hat{n} denotes the length of the sequence after compression. Assuming the length of the text tokens is l and the anchor ratio is λ , then we can get:

$$\text{IKOD_FLOPs} = L \times (24nd^2 + 4n^2d) + L \times (24\hat{n}d^2 + 4\hat{n}^2d), \quad (14)$$

$$\hat{n} = (n - l) + \lambda \times l = n + (\lambda - 1)l. \quad (15)$$

We define the FLOPs growth rate as follows:

$$\begin{aligned} g &= \frac{\text{IKOD_FLOPs} - \text{Original_FLOPs}}{\text{Original_FLOPs}} \\ &= \frac{\text{IKOD_FLOPs}}{\text{Original_FLOPs}} - 1. \end{aligned} \quad (16)$$

Combine Eq.13-16, we obtain:

$$g = 1 - \frac{2n - (1 - \lambda)l + 6d}{6nd^2 + n^2}(1 - \lambda)l, \quad (17)$$

Since $0 < 1 - \lambda < 1$ and $l < n$, we conclude that $g < 1$ based on Eq.17, and we can use g to roughly estimate the proportion of the increase in inference cost.

J Case Studies

We leverage CHAIR evaluations as case studies to qualitatively compare the decoding outputs of IKOD with other methods. Responses generated by IKOD and other decoding methods including OPERA, VCD, HALC and AGLA incorporating LLaVA-1.5 and InstructBLIP backbones are demonstrated in Figure 10 and 11, respectively. In all plots, red fonts indicate the hallucinated contents, including any of object existence, attribute or relationship hallucinations. We can see that IKOD effectively mitigates object hallucinations without loss of details, which is consistent with the results in Table 2.



OPERA: The image features a brown and white horse standing next to a horse-drawn carriage. The horse is positioned on the left side of the carriage, while the carriage is on the right side. The horse appears to be wearing a harness, indicating that it is ready to pull the carriage.
In addition to the horse and carriage, there are two people visible in the scene. One person is standing closer to the left side of the horse, while the other person is positioned near the right side of the carriage.

IKOD: The image features a brown horse pulling a red carriage with a white wheel. The horse is standing on a dirt road, and the carriage is parked next to a building. The horse is wearing a harness, and the carriage is attached to the horse's harness, indicating that it is being used for transportation. The horse and carriage are positioned in the foreground, and the scene is set in a dirt-covered area, creating a unique and picturesque setting.

HALC: The image features a brown horse with a white face, standing on a road next to a carriage. The horse is wearing a harness and appears to be pulling the carriage. The carriage is red and white, and it is positioned behind the horse.
There are two people in the scene, one standing closer to the horse and the other further away. The person near the horse seems to be attending to the horse or the carriage, while the other person is standing further back, possibly observing the scene or waiting for their turn to ride in the carriage.

VCD: The image features a brown horse standing next to a red carriage, which is being used as a horse-drawn carriage. The horse is wearing a harness and is pulling the carriage, creating a picturesque scene. The carriage is large and spacious, providing ample room for the passengers.
In the background, there are a few trees, adding to the overall ambiance of the scene. The horse and carriage are the main focus of the image, showcasing the traditional mode of transportation.

AGLA: The image features a brown horse standing on a road, pulling a carriage with a red and white color scheme. The horse is positioned in the center of the scene, with the carriage behind it. The carriage has a bench seat, and the horse is wearing a harness, indicating that it is ready for a ride.
In addition to the horse and carriage, there are two people visible in the scene. One person is standing near the left side of the horse, while the other person is located on the right side of the horse. The presence of these individuals suggests that they might be passengers or caretakers of the horse and carriage.



OPERA: The image features a brown and white dog skillfully riding a skateboard down a street. The dog appears to be enjoying the ride and is the main focus of the scene.
Several people are watching the dog from various positions along the street. Some are standing closer to the dog, while others are further away, observing the unique sight. A chair can be seen in the background, possibly belonging to one of the onlookers.
In addition to the people and the dog, there are a couple of handbags visible in the scene, likely belonging to some of the spectators.

IKOD: The image features a brown and white dog skillfully riding a skateboard down a street, likely in a parade or a street event. The dog is the center of attention, as it appears to be the main attraction for the crowd of people watching the dog skate. There are several people in the scene, with some of them standing near the dog and others watching from a distance.
The crowd is spread out, with some standing close to the dog and others standing further back, observing the spectacle. The dog and the skateboard are positioned in the center of the scene, capturing the audience's attention and creating a lively atmosphere.

HALC: The image features a brown and white dog skillfully riding a skateboard down a street. The dog appears to be enjoying the ride, and it is the main focus of the scene.
There are several people watching the dog's performance, with some standing closer to the dog and others further away. A few chairs are scattered around the area, possibly for the spectators to sit and enjoy the show. Additionally, there are a couple of umbrellas in the scene, one near the left side and another towards the right side, possibly providing shade for the onlookers.

VCD: The image features a brown and white dog skillfully riding a skateboard down a street. The dog appears to be enjoying the ride, and it is the main focus of the scene.
There are several people watching the dog from various positions along the street. Some are standing closer to the dog, while others are further away. A few chairs are scattered around the scene, with one near the left side of the image and another on the right side.
In addition to the people and chairs, there are a couple of handbags placed on the ground, one near the center of the image and the other closer to the right side.

AGLA: The image features a brown and white dog skillfully riding a skateboard down a street. The dog appears to be enjoying the ride, and it is the main focus of the scene.
There are several people watching the dog's performance from various positions around the street. Some are standing closer to the dog, while others are further away. A few chairs can be seen scattered around the area, possibly for spectators to sit and enjoy the show.
In addition to the people and chairs, there are a couple of handbags placed on the ground, possibly belonging to the onlookers. The overall atmosphere seems lively and entertaining as the dog showcases its talent on the skateboard.

Figure 10: Two examples of generated captions by different decoding methods with LLaVA-1.5 backbone.



OPERA: The image depicts a spacious room with a wooden bench placed in front of a staircase. The bench is positioned near the bottom of the staircase, creating a cozy and inviting atmosphere. There are two paintings hanging on the wall above the bench, adding a touch of artistic flair to the space. In addition to the bench and paintings, **there are several potted plants scattered throughout the room, giving it some greenery and life.** A vase can be seen on the left side of the room, adding a decorative element to the space. Overall, the room exudes a warm and welcoming ambiance, perfect for relaxation or socializing.

IKOD: The image features a long wooden bench placed in a room with a white wall and a stairway. The bench is placed in the center of the room, with a few steps leading up to the stairway. There are two paintings on the wall, one on the left and one on the right side of the stairway, adding to the room's aesthetic. The bench and the paintings are positioned in the room, creating a cozy and artistic atmosphere.

VCD: The image features a long wooden bench placed in a room with a white wall and a staircase. The bench is situated in the middle of the room, **with a potted plant placed on the left side of the bench.** There are two paintings hanging on the wall, one on the left side and the other on the right side of the room. The paintings are positioned close to the bench, with one on the left and the other on the right side of the bench. The room has a spacious feel, with a lot of space between the bench and the paintings.

HALC: The image features a narrow staircase leading up to the second floor of an office building. Alongside the stairs, there is a wooden bench placed against the wall. A painting can be seen on one side of the room, while another painting hangs above the staircase landing. **Two potted plants are also present in the scene, with one located near the bottom left corner and the other towards the top right corner.** These elements create a cozy atmosphere within the space.

AGLA: The image features a long wooden bench placed in a room with a staircase. The bench is situated near the staircase, with a painting on the wall above it. There are two paintings on the wall, one on the left and one on the right side of the room. The bench is positioned in the center of the room, **with a potted plant placed on the left side of the bench.** The room has a clean and organized appearance, with a sense of elegance and sophistication.



OPERA: The image features a young boy sitting on a set of stairs, holding a tennis racket. He is wearing a red hoodie and jeans, and appears to have a big smile on his face. The tennis racket is positioned close to the boy, indicating that he is ready to play or practice with it. There are several other objects in the scene, **including a backpack and a handbag placed on the floor near the stairs.** Additionally, a pair of shoes can be seen on the right side of the image.

IKOD: The image features a young boy sitting on a set of stairs, holding a tennis racket. He is wearing a red jacket and jeans, and appears to be in a happy and excited state. The tennis racket is positioned in his hand, ready to be used for a fun game or practice session. The boy is sitting on the stairs, and the tennis racket is placed in his hand, making it a great moment captured in the scene.

HALC: The image features a young boy sitting on the stairs, holding a tennis racket. He is wearing a red jacket and jeans, and appears to be enjoying his time playing with the tennis racket. **A person can also be seen in the background, possibly accompanying the child or watching him play.** There are several other objects scattered around the scene, including two shoes placed near the steps, **one at the bottom of the staircase and another closer to the top. Another shoe can be found further up the stairs, close to the railing.** Additionally, **there is a handbag located towards the right side of the image, likely belonging to someone nearby.**

VCD: The image features a young child sitting on a set of stairs, holding a tennis racket. The child is wearing a red jacket and jeans, and appears to be enjoying the moment. The tennis racket is positioned close to the child, and there is a shoe placed near the child's left foot. The scene is set in a house, **with a chair placed nearby.**

AGLA: The image features a young boy sitting on a set of stairs, holding a tennis racket. He is wearing a red jacket and jeans, and appears to be enjoying the moment. The tennis racket is positioned close to the boy, and there are several other objects scattered around the scene, **including a backpack and a shoe.** The overall atmosphere is casual and relaxed, with the boy seemingly content with his tennis racket.

Figure 11: Two examples of generated captions by different decoding methods with InstructBLIP backbone.